ISSN 1027-4510, Journal of Surface Investigation: X-ray, Synchrotron and Neutron Techniques, 2021, Vol. 15, No. 5, pp. 920–926. © Pleiades Publishing, Ltd., 2021.
Russian Text © The Author(s), 2021, published in Poverkhnost', 2021, No. 9, pp. 32–39.

# Synthesis of the Metal-Organic Framework UiO-66 in the Form of Nanoparticles with a Modified Surface

**V. V. Butova[a, *], O. A. Burachevskaya[a], P. V. Medvedev[a], I. E. Gorban[a], A. A. Kuzharov[a], D. B. Trushina[b, c], and M. A. Soldatov[a]**

[a] *The Smart Materials Research Institute, Southern Federal University, Rostov-on-Don, 344090 Russia*

[b] *Shubnikov Institute of Crystallography FSRC "Crystallography and Photonics," Russian Academy of Sciences, Moscow, 119333 Russia*

[c] *Sechenov First Moscow State Medical University, Moscow, 119991 Russia*

**e-mail: vbutova@sfedu.ru*

Received January 27, 2021; revised February 14, 2021; accepted February 20, 2021

**Abstract**—We report on a synthesis procedure for obtaining a UiO-66 metal-organic framework in the form of nanoparticles with a modified surface. A distinctive feature of the developed procedure is that modification occurs directly during synthesis. Biocompatible polyethylene glycol (PEG) is selected as the organic polymer covering the surface of the UiO-66 nanoparticles. The effect of the degree of PEG polymerization on the size, morphology, and surface charge of UiO-66 nanoparticles is studied. The presence of PEG molecules is confirmed by infrared (IR) spectroscopy. The materials obtained are single phase and characterized by a high degree of crystallinity. The particle size varies from 80 to 120 nm, depending on the type of PEG used. A high surface charge in an aqueous medium (ζ-potential over 20 mV) indicates the possibility of forming a stable suspension. Thus, the obtained materials are promising as nanocontainers for the delivery of biologically active substances.

**Keywords:** metal-organic frameworks, metal-organic coordination polymers, polyethylene glycol, drug delivery, nanocontainers, porous nanoparticles

**DOI:** 10.1134/S1027451021050037

## INTRODUCTION

Metal-organic frameworks (MOFs) are a class of porous materials with a modular structure [1, 2]. Their structure can be thought of as a combination of organic and inorganic constituents linked by covalent bonds. The inorganic parts are clusters of metals coordinated by oxygen or nitrogen (less often by other nonmetals). The organic molecules linking these clusters into a single framework are called linkers [3]. Thus, the size, shape, and functionality of the pores of MOFs are determined by a combination of organic and inorganic components, which opens up wide possibilities for creating materials with desired properties. This structure flexibility makes it possible to use MOFs in a wide variety of areas: for the storage and separation of gases, selective catalysis, and water and air purification as part of chemical current sources [4, 5]. The material properties must be selected for each task. Recently, great success has been achieved in the application of MOFs for biomedical problems, in particular, for targeted drug delivery. The critical properties for this application are the nanoscale size, stability, and low toxicity of MOFs.

One of the types of MOFs that meets these requirements is UiO-66. It consists of zirconium-oxygen clusters connected by terephthalic-acid molecules into a three-dimensional cubic framework (Fig. 1). Each cluster is formed by six zirconium ions connected by bridging OH-groups ($\mu_3$-OH), which can split off hydrogen, transforming into bridging oxygen ($\mu_3$-O). The composition of the cluster changes according to the following scheme: $Zr_6O_4(OH)_4^{12+} \rightarrow Zr_6O_6^{12+}$. Each zirconium-oxygen cluster is coordinated by 12 linker molecules. This high bonding, together with strong covalent Zr–O bonds, results in a chemically and thermally stable material. The UiO-66 framework contains two types of pores (tetrahedral and octahedral) and has a high specific surface area (1125 $m^2/g$) [6].

To obtain UiO-66 in the form of nanoparticles, the method of coordination modulators is usually used. According to this method, an additional monocarboxylic or inorganic acid is added to the reaction mixture [7–9]. Benzoic, hydrochloric or acetic acids are most often used as modulators. Acetic acid was used to prepare UiO-66 nanoparticles in [10], which were then

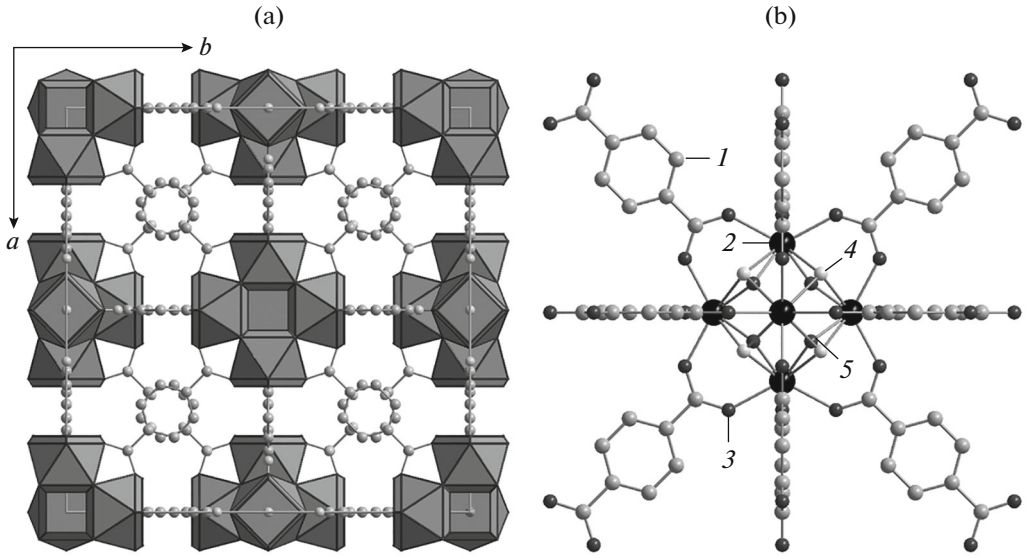


**Fig. 1.** Model of the structure of UiO-66: (a) cubic unit cell (zirconium-oxygen polyhedra are shown, the spheres are carbon atoms); (b) model of a zirconium-oxygen cluster coordinated by terephthalic-acid molecules ((*1*) carbon, (*2*) zirconium, and (*3*) oxygen atoms, both variants of the (*4*) $\mu_3$-OH and (*5*) $\mu_3$-O bridging groups are shown).

modified with polyvinylpyrrolidone so that they could be combined into two-dimensional layers. A UiO-66 derivative with an azide fragment was obtained using the same modulator [11]. The surface of the particles was further coated with DNA molecules, which increased the stability of the colloid in saline and increased cellular uptake compared to unmodified particles. In [12], UiO-66 nanoparticles were obtained; benzoic and hydrochloric acids simultaneously acted as modulators. Then the nanoparticles were used for postsynthetic exchange; linkers were replaced with molecules of photosensitizers and the resulting material was used in photodynamic therapy.

Coating the surface of MOF crystals with biopolymers can significantly improve their properties. Thus, coating the UiO-66 surface with polyethylene glycol (PEG) made it possible to achieve the controlled release of a model fluorescent dye. At pH 7.4, PEG chains block the interaction of the medium with the nanoparticle surface, while at pH 5.5 the loaded molecules are released. In addition, PEG coating resulted in increased uptake of the material by cells [13]. In [14], a radioactive analogue: UiO-66 with the $^{89}$Zr isotope, emitting positrons, is reported. The surface of the nanoparticles was additionally functionalized with PEG with a pyrene group and conjugated to a peptide ligand for accumulation in breast tumors. The porous framework of UiO-66 was saturated with doxorubicin, which served as both a therapeutic agent and a fluorescence imager in this study.

In this work, a procedure is presented that makes it possible to obtain UiO-66 in the form of nanoparticles, the surface of which is modified with PEG, so, synthesis and modification occur simultaneously.

## EXPERIMENTAL

### *Synthesis*

The initial reagents $ZrCl_4$, terephthalic acid (BDC), dimethylformamide (DMF), isopropyl alcohol ($CH_3CH(OH)CH_3$) manufactured by Alfa Aesar were used without additional purification. Also, polyethylene glycols (PEG) with an average molecular weight of 200 (PEG200), 600 (PEG600), and 1500 (PEG1500) from Sigma-Aldrich were used. Deionized water was obtained from distilled water in a Simplicity UV purification system.

To obtain an unmodified UiO-66 sample, a method developed earlier by the authors was chosen, which makes it possible to obtain MOF in the form of nanoparticles [15]. For this, an additive of benzoic acid was used, which acts as a modulator. Modified samples were obtained by the same method, but with the addition of PEG. Zirconium tetrachloride (0.1507 g) was dissolved in DMF (15 mL), 35 μL of water was added, and then benzoic acid (0.7890 g) was added and stirred with a magnetic stirrer until complete dissolution. Then the corresponding PEG was added to the resulting clear solution (Table 1). The latter terephthalic acid (0.1073 g) was added to the reaction mixture, stirred until complete dissolution, and placed in an oven preheated to 120°C for 24 h. The resulting powders were separated by centrifugation, thoroughly washed with DMF, isopropanol, and then dried at 60°C in air for 16 h.

## ANALYSIS PROCEDURES

Diffraction patterns were obtained on a Bruker D2 PHASER X-ray powder diffractometer with a copper

**Table 1.** Designations of samples and molar ratios of precursors used for their preparation

| Sample | Molar ratio of precursors | | | | | | |
|---|---|---|---|---|---|---|---|
| | $ZrCl_4$ | BDC | water | PEG200 | PEG600 | PEG1500 | DMF |
| UiO-66 | 1 | 1 | 3 | – | – | – | 300 |
| 200 | | | | 5 | – | – | |
| 600 | | | | – | 5 | – | |
| 1500 | | | | – | – | 5 | |

anode (Cu$K_\alpha$, $\lambda = 1.5417$ Å) in the 2θ range from 5° to 50° with a step of $2\theta = 0.01°$. The infrared (IR) spectra were measured on a Bruker Vertex 70 spectrometer in the ATR (Attenuated Total Reflectance) geometry using an MCT detector and a Bruker Platinum ATR attachment. The spectra were measured in the range from 5000 to 300 $cm^{-1}$ with a resolution of 1 $cm^{-1}$ over the course of 64 scans. The comparison sample was air. Transmission electron microscopy (TEM) images were obtained using an FEI Tecnai G2 Spirit TWIN microscope with an accelerating voltage of 80 kV. The $Z$ potential and pH values of the suspensions were measured using a Stabino ζ-potential analyzer (particle charge titrator) to analyze the stability of colloidal particles and suspensions. To prepare a suspension, the corresponding powder sample (0.02 g) was placed in 10 mL of deionized water or saline solution and then homogenized for 30 min in an ultrasonic bath. The particle size in the suspension was determined using a NANO-flex analyzer based on the theory of dynamic light scattering. Nitrogen-adsorption measurements were performed using the ASAP 2020 system for determining the surface area and measuring the porosity of solid materials (Micrometrics, USA). The Brunauer–Emmett–Teller model was used to calculate the specific surface area.

## RESULTS AND DISCUSSION

The X-ray diffraction patterns are shown in Fig. 2. As one can see from the data presented, the addition of PEG during synthesis has no noticeable effect on the phase composition and degree of crystallinity of the samples. All profiles can be described in terms of cubic symmetry, space group $Fm\bar{3}m$ (No. 225). The unit-cell parameters of the UiO-66, 200, 600, and 1500 samples are close and amount to 20.7589(4), 20.7140(16), 20.7700(6), and 20.7659(7) Å, respectively.

According to the TEM images (Fig. 3), the shape of the particles is retained regardless of the introduced PEG. Thus, the UiO-66 sample is made up of octahedral crystals, which corresponds to published data. Samples 200 and 600 are also represented by octahedral particles; however, one can see that the crystal faces are smoothed, which may indicate the formation of an amorphous PEG layer on the surface of the particles. All three UiO-66, 200, and 600 samples show a low degree of aggregation. In contrast, sample 1500 is represented by large aggregates consisting of octahedral crystals.

It can also be observed that the introduction of PEG during synthesis leads to a change in the average particle size. The average particle size in the UiO-66 sample obtained without the introduction of PEG was 66 nm. The introduction of PEG200 and PEG600 during synthesis slightly increases the average particle size, but they remain monodisperse (Fig. 4). The average particle size in samples 200 and 600 according to TEM data was 78 and 91 nm. The increase in particle size is in good agreement with surface modification by polymer molecules. Molecules with a longer carbon chain lead to a larger increase in the average particle size. Unlike UiO-66, 200, and 600 samples, sample 1500 prepared with PEG1500 polymer exhibits not only a larger particle size, but also a wider particle size distribution. The average particle size of sample 1500 was 117 nm. The particle size determined by dynamic light scattering is larger than the size obtained by TEM (Fig. 4c). This is due to the measurement procedure, which is sensitive to the formation of aggregates and

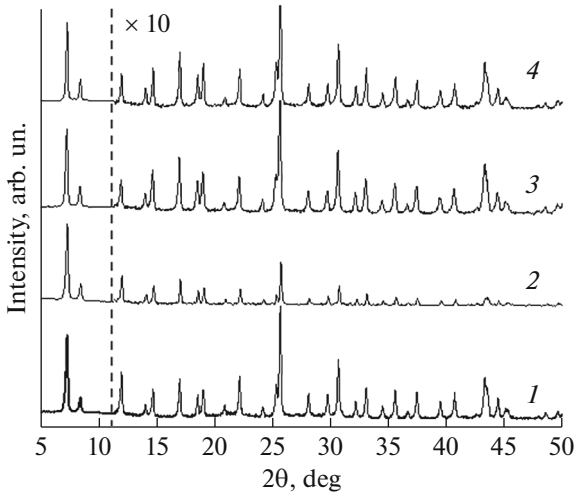


**Fig. 2.** Diffraction patterns of (*1*) UiO-66, (*2*) 200, (*3*) 600, and (*4*) 1500 samples. Profiles are *y* shifted and multiplied by 10 after the dashed intensity line to better represent the data.

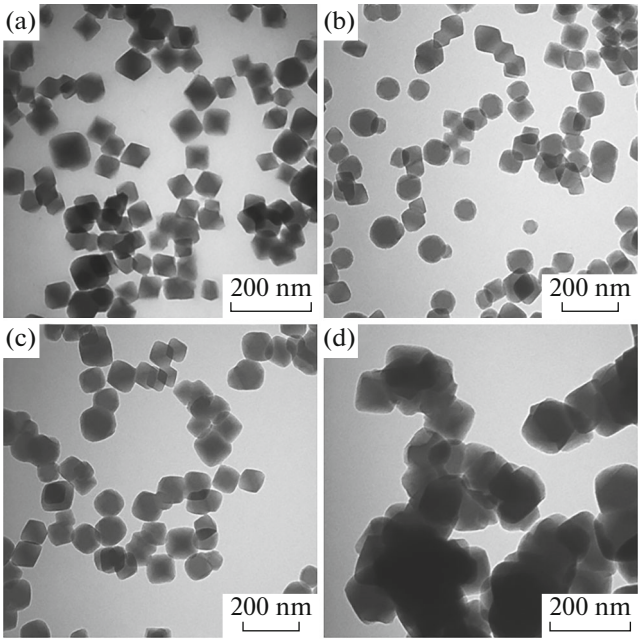


**Fig. 3.** TEM images of (a) UiO-66, (b) 200, (c) 600, and (d) 1500 samples.

solvation shells. However, the trend persists, i.e., with an increase in the molecular weight of PEG, the particle size increases. The average particle size in an aqueous suspension according to dynamic-light-scattering data was 180, 210, and 355 nm for samples 200, 600, and 1500, respectively. The average particle size in the initial UiO-66 sample is 200 nm. It can be assumed that the coating with polyethylene glycol reduces the degree of aggregation and the thickness of the solvation shell of the particles.

To measure the acidity and ζ potential of the samples, the suspension was prepared in water and saline. The acidity of the suspensions for each sample did not change significantly both in water and in saline, and the medium had a noticeable effect on the values of the ζ potential. Suspension UiO-66 is rather acidic. This is due to the structure of the zirconium-oxygen clusters that form the crystal lattice of the MOF. The zirconium ions in it are linked by bridging $\mu_3$-OH groups, which determine the acidic properties of the entire material ($pK_a$ = 3.52) [16, 17]. When MOF is modified with PEG molecules, the pH of the medium increases from 3 for unmodified UiO-66 to 4.5–5.5 for samples 200, 600, and 1500. Since PEG itself is a weak acid and cannot significantly affect the acidity value, such pH changes can be explained by modification of the crystal surface. The polymer molecules partially block access to the acidic $\mu_3$-OH groups of the initial MOF, which reduces its acidic properties.

The coating of MOF crystals with PEG molecules also confirms the change in the ζ potential (Fig. 5). As one can see from the diagram, surface modification

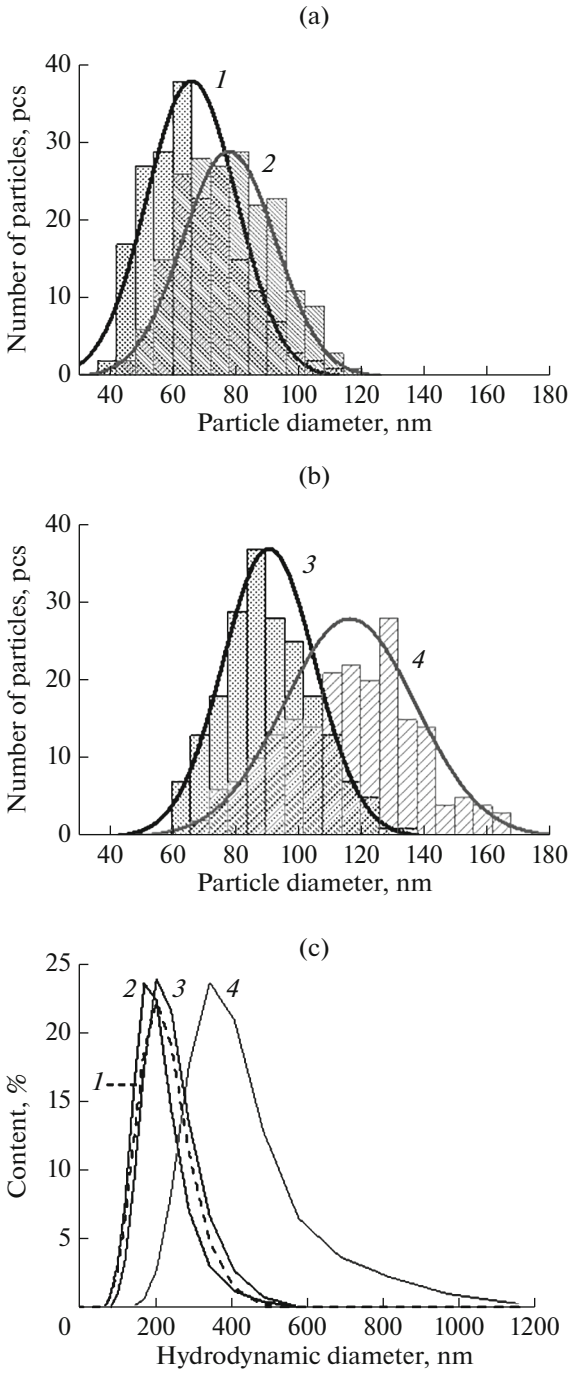


**Fig. 4.** Particle size distribution obtained from TEM data for 200 particles in each sample (a, b) and by dynamic light scattering in an aqueous suspension (c) for samples: (a) UiO-66 (*1*), 200 (*2*); (b) 600 (*3*), 1500 (*4*); (c) UiO-66 (*1*), 200 (*2*), 600 (*3*), 1500 (*4*).

leads to a decrease in the value of the ζ potential from 41 mV for UiO-66 to 21, 26, and 27 mV for samples 200, 600, and 1500 in an aqueous medium, respectively. In saline, the tendency is the same: the ζ potential decreases from 3 mV for UiO-66 to 2 mV for modified samples. The high ζ potential of UiO-66 in water

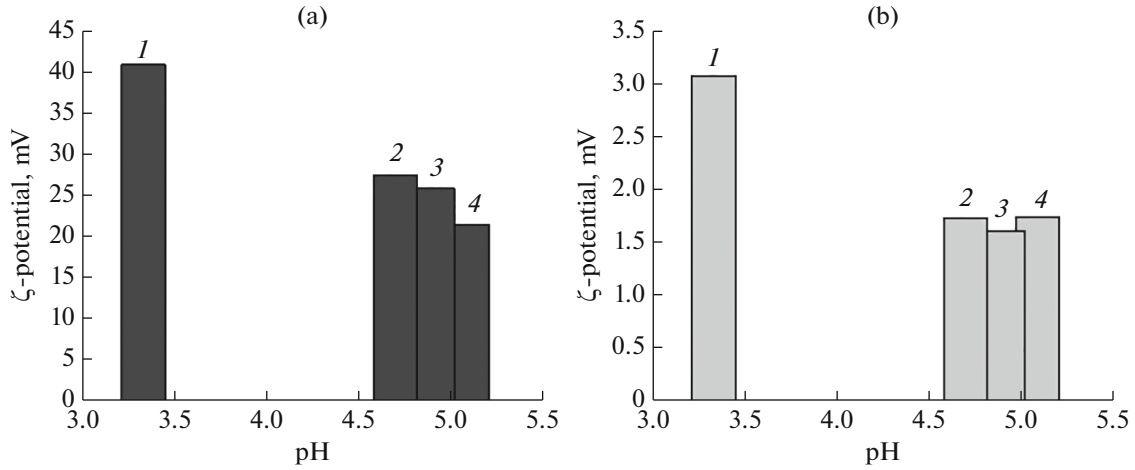


**Fig. 5.** Diagram showing the change in pH and ζ potential of a suspension of the synthesized samples (*1*) UiO-66, (*2*) 1500, (*3*) 600, and (*4*) 200 in (a) an aqueous medium and in (b) saline.

is primarily associated with the deprotonation of zirconium clusters [16]. Hydrogen ions that formed during the dissociation of $\mu_3$-OH groups and cause low pH values of the UiO-66 suspension form a double layer on the surface of the negatively charged framework. Accordingly, the decrease in the surface charge is in good agreement with the decrease in the availability of $\mu_3$-OH groups after modification of the PEG surface. However, in general, high values of the ζ potential in an aqueous medium are an indicator of the stability of a colloidal solution. When passing to suspensions in saline, a decrease in the ζ potential is observed while maintaining pH values. This is apparently due to the effect of additional $Na^+$ and $Cl^-$ ions in the solution, which affects the double layer [18].

The IR spectra of all synthesized samples were measured (Fig. 6). In the "fingerprint" region, the spectra are identical, since this range is due to vibrations of the UiO-66 framework. The peaks at 505 and 550 $cm^{-1}$ are attributed to the vibrations of the bonds of zirconium with carboxyl groups of the linker [6]. A small peak at 613 $cm^{-1}$ can be attributed to the deformation vibrations of benzene rings of linkers. The peak at 740 $cm^{-1}$ is due to vibrations of the C–H and O–H groups [15]. Symmetric and asymmetric vibrations of carboxyl groups give peaks at 1390 and 1585–1660 $cm^{-1}$, respectively [19]. Benzoic acid used in the synthesis of MOF remains in the structure and gives peaks at 720 and 1020 $cm^{-1}$ [15]. Passing to the region of 2500–3900 $cm^{-1}$, one can note the differences in the spectra of the modified and the initial samples. The broad peak at 3000–3600 $cm^{-1}$ is attributed to water adsorbed in the pores. The peak at 3675 $cm^{-1}$ common for all spectra is attributed to the vibrations of free

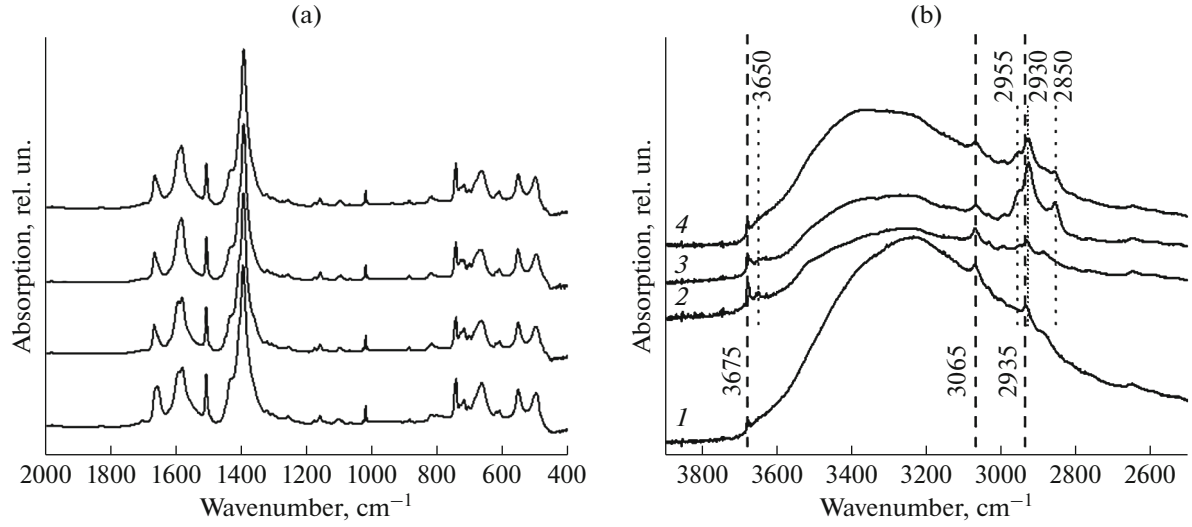


**Fig. 6.** IR spectra of samples (*1*) UiO-66, (*2*) 200, (*3*) 600, and (*4*) 1500 in the range: (a) 400–2000; (b) 2500–3900 $cm^{-1}$.

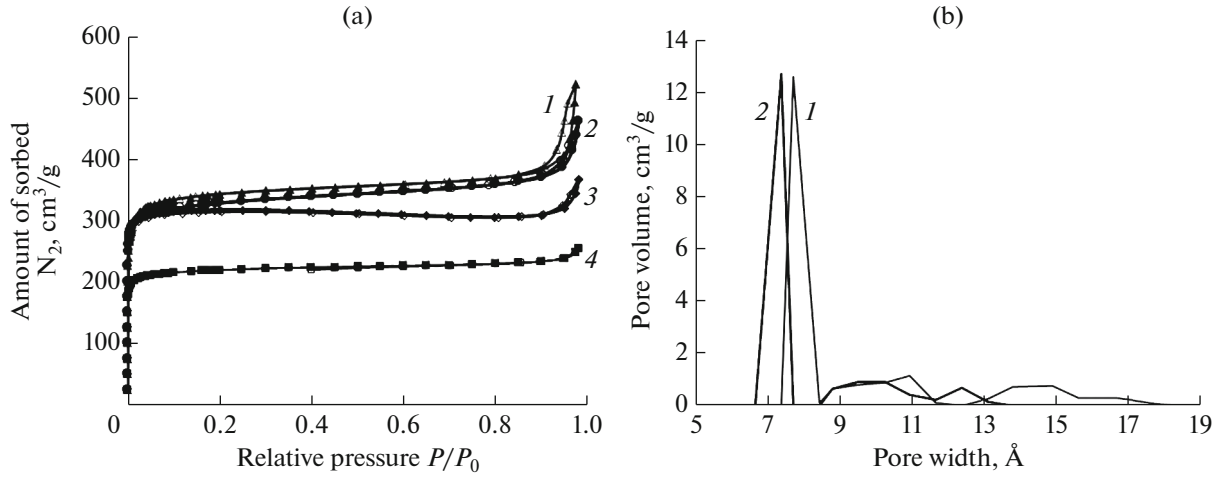


**Fig. 7.** Isotherms of the adsorption–desorption of nitrogen (a) for samples (*1*) UiO-66, (*2*) 200, (*3*) 600, and (*4*) 1500; filled symbols denote adsorption branches; empty shows the desorption branches. Pore size distribution (b) of samples (*1*) UiO-66 and (*2*) 200, calculated using density functional theory according to the model of cylindrical pores.

$\mu_3$-bridging hydroxyls belonging to zirconium clusters [19, 20]. The peaks at 3065 and 2935 $cm^{-1}$ refer to the vibrations of C–H bonds and are common for all samples [20]. The spectra of samples 200, 600, and 1500 contain new peaks that were not observed for the UiO-66 sample and are due to the presence of a PEG layer covering the particles. Thus, the peaks at 3650 and 2955 $cm^{-1}$ refer to hydroxyl groups linked by hydrogen bonds, the peaks at 2930 and 2850 $cm^{-1}$ are due to vibrations of the $CH_2$-groups of PEG [21].

For the successful application of materials in the biomedical field, it is also necessary to maintain the availability of pores for guest molecules. To confirm the high porosity of the modified MOFs, nitrogen adsorption–desorption isotherms were measured (Fig. 7a). The isotherms of samples 200, 600, and 1500 have a similar shape to UiO-66. It can be classified as type I according to the IUPAC classification. This shape is typical for microporous materials. The specific surface areas of the UiO-66, 200, 600, and 1500 samples were 1355, 1295, 1285, and 880 $m^2/g$. Thus, there is a slight decrease in the porosity of samples 200 and 600 in comparison with unmodified UiO-66, while for sample 1500 there is a decrease in porosity by 35%. In addition, a slight decrease in the pore diameter of sample 200 compared to UiO-66 can be seen in the pore size distribution. This indicates that the pore surface is decorated with PEG molecules (Fig. 7b).

## CONCLUSIONS

In the course of this study, a method for the synthesis of UiO-66 was developed, which makes it possible to obtain nanoparticles of MOCP with a modified surface. PEGs with an average molecular weight of 200, 600, and 1500 were used as modifying polymers. It was shown that the introduction of these polymers does not lead to a change in the phase composition or the degree of crystallinity of the product. However, depending on the degree of PEG polymerization, the average particle size changes, namely, an increase in the molecular weight of PEG leads to an increase in the particle size from 80 to 120 nm. IR spectroscopy confirmed the presence of PEG molecules in samples 200, 600, and 1500. It was shown that surface modification with PEG molecules reduces the availability of $\mu_3$-OH groups of zirconium clusters of the UiO-66 framework. This leads to a decrease in the concentration of hydrogen ions in aqueous suspensions and a decrease in the $\zeta$ potential. However, its value is still high, which makes it possible to expect the formation of a stable colloidal solution. Thus, the developed procedure can be used to obtain biocomposites or containers for drugs based on modified porous UiO-66 nanoparticles.

## FUNDING

The study was supported by the Russian Science Foundation, project no. 19-73-10069.

## REFERENCES

1. V. V. Butova, M. A. Soldatov, A. A. Guda, K. A. Lomachenko, and C. Lamberti, Russ. Chem. Rev. **85**, 280 (2016). https://doi.org/10.1070/RCR4554
2. O. M. Yaghi, M. O'Keeffe, N. W. Ockwig, H. K. Chae, M. Eddaoudi, and J. Kim, Nature **423**, 705 (2003). https://doi.org/10.1038/nature01650
3. D. J. Tranchemontagne, J. L. Mendoza-Cortes, M. O'Keeffe, and O. M. Yaghi, Chem. Soc. Rev. **38**, 1257 (2009). https://doi.org/10.1039/B817735J

4. S. Bai, X. Liu, K. Zhu, S. Wu, and H. Zhou, Nat. Energy **1**, 16094 (2016). https://doi.org/10.1038/nenergy.2016.94
5. W. Li, S. Hu, X. Luo, Z. Li, X. Sun, M. Li, F. Liu, and Y. Yu, Adv. Mater. **29**, 1605820 (2017). https://doi.org/10.1002/adma.201605820
6. V. V. Butova, K. S. Vetlitsyna-Novikova, I. A. Pankin, K. M. Charykov, A. L. Trigub, and A. V. Soldatov, Microporous Mesoporous Mater. **296**, 109998 (2020). https://doi.org/10.1016/j.micromeso.2020.109998
7. C. Atzori, G. C. Shearer, L. Maschio, B. Civalleri, F. Bonino, C. Lamberti, S. Svelle, K. P. Lillerud, and S. Bordiga, J. Phys. Chem. C **121**, 9312 (2017). https://doi.org/10.1021/acs.jpcc.7b00483
8. V. V. Butova, A. P. Budnyk, A. A. Guda, K. A. Lomachenko, A. L. Bugaev, A. V. Soldatov, S. M. Chavan, S. Øien-Ødegaard, U. Olsbye, K. P. Lillerud, C. Atzori, S. Bordiga, and C. Lamberti, Crystal Growth Des. **17**, 5422 (2017). https://doi.org/10.1021/acs.cgd.7b00892
9. A. Schaate, P. Roy, A. Godt, J. Lippke, F. Waltz, M. Wiebcke, and P. Behrens, Chem.-Eur. J. **17**, 6643 (2011). https://doi.org/10.1002/chem.201003211
10. G. Lu, C. Cui, W. Zhang, Y. Liu, and F. Huo, Chem.—Asian J. **8**, 69 (2013). https://doi.org/10.1002/asia.201200754
11. W. Morris, W. E. Briley, E. Auyeung, M. D. Cabezas, and C. A. Mirkin, J. Am. Chem. Soc. **136**, 7261 (2014). https://doi.org/10.1021/ja503215w
12. W. Wang, L. Wang, Z. Li, and Z. Xie, Chem. Commun. **52**, 5402 (2016). https://doi.org/10.1039/c6cc01048b
13. I. Abánadez Lazaró, S. Haddad, S. Sacca, C. Orellana-Tavra, D. Fairen-Jimenez, and R. S. Forgan, Chem **2**, 561 (2017). https://doi.org/10.1016/j.chempr.2017.02.005
14. D. Chen, D. Yang, C. A. Dougherty, W. Lu, H. Wu, X. He, T. Cai, M. E. Van Dort, B. D. Ross, and H. Hong, ACS Nano **11**, 4315 (2017). https://doi.org/10.1021/acsnano.7b01530
15. V. V. Butova, O. A. Burachevskaya, I. V. Ozhogin, G. S. Borodkin, A. G. Starikov, S. Bordiga, A. Damin, K. P. Lillerud, and A. V. Soldatov, Microporous Mesoporous Mater. **305**, 110324 (2020). https://doi.org/10.1016/j.micromeso.2020.110324
16. A. H. Ibrahim, W. A. El-Mehalmey, R. R. Haikal, M. E. A. Safy, M. Amin, H. R. Shatla, S. G. Karakalos, and M. H. Alkordi, Inorg. Chem. **58**, 15078 (2019). https://doi.org/10.1021/acs.inorgchem.9b01611
17. R. C. Klet, Y. Liu, T. C. Wang, J. T. Hupp, and O. K. Farha, J. Mater. Chem. A **4**, 1479 (2016). https://doi.org/10.1039/c5ta07687k
18. G. V. Lowry, R. J. Hill, S. Harper, A. F. Rawle, C. O. Hendren, F. Klaessig, U. Nobbmann, P. Sayre, and J. Rumble, Environ. Sci.: Nano **3**, 935 (2016). https://doi.org/10.1039/c6en00136j
19. V. V. Butova, A. P. Budnyk, K. M. Charykov, K. S. Vetlitsyna-Novikova, A. L. Bugaev, A. A. Guda, A. Damin, S. M. Chavan, S. Øien-Ødegaard, K. P. Lillerud, A. V. Soldatov, and C. Lamberti, Inorg. Chem. **58**, 1607 (2019). https://doi.org/10.1021/acs.inorgchem.8b03087
20. K. Chakarova, I. Strauss, M. Mihaylov, N. Drenchev, and K. Hadjiivanov, Microporous Mesoporous Mater. **281**, 110 (2019). https://doi.org/10.1016/j.micromeso.2019.03.006
21. R. Xu, Z. Wang, M. Wang, Z. Qiao, and J. Wang, J. Membr. Sci. **573**, 455 (2019). https://doi.org/10.1016/j.memsci.2018.12.027

*Translated by V. Kudrinskaya*